# Speed Control of Three-Wheel Electric Scooter with Fuzzy Logic Control

Chergui Hicham*, Abdelfatah Nasri*, ‡Korhan Kayisli**

*SGRE Laboratory, Tahri Mohamed Bechar University, B.P 417, 08000, Bechar, ALGERIA

**Department of Electric Electronics, Faculty of Engineering, Nisantasi University, 34310, Istanbul, TURKEY

(chergui4510@gmail.com, nasriab1978@yahoo.fr, korhankayisli@gmail.com)

‡ Corresponding Author; Korhan Kayisli, Nisantasi University, Sariyer, ISTANBUL, Tel: +90 212 210 10 10

korhankayisli@gmail.com

*Received: 15.07.2019 Accepted:17.08.2019*

**Abstract-** At the last decade, a growing number of electric scooters appeared on the world market as a key to solve mobility problems in the crowded cities. The main purpose of this paper is to design a three-wheeled electric scooter with protracted autonomy. This model is driven by double BLDCM positioned on the back wheels and controlled by a fuzzy logic controller. The scooter contains an electronic differential system that provides robust control of the scooter and it also allows each drive wheel to be separately controlled to rotate at different speeds. The proposed controller of electric scooter system is simulated with MATLAB Simulink environment. The findings of simulation show the effectiveness of the suggested supervision.

**Keywords** Electric scooter, Electronic differential, BLDCM, Fuzzy logic controller.

## 1. Introduction

The technologies about the electrical vehicles have been advanced day by day and there are many researches have been performed about this area. However, to achieve the high density storage systems for electrical energy has not been solved yet. Nowadays, the only convenient solution seems to be the implementation of hybrid electric vehicles, whether internal combustion engines or fuel cell engines, which in all cases entails increased costs and complexity. Additionally, due to only electric vehicles usage does not provide increased autonomy, the vehicles such as scooters are generally dedicated to urban areas. The benefits of the scooter usage become significant in large urban areas due to much traffic with large numbers of the vehicles.

Unfortunately, the preceding prototypes could not provide the same speed and the required acceleration in the same area. The requirement for electric scooters have widespread usage in the world and called as an immediate electric counterpart [1, 3, 8]. In this study, the solution for better performance of a three-wheeled electric scooter is presented. This prototype propelled by BLDCM includes Hall Effect Sensors and these motors are placed on the rear wheels with a fuzzy logic controller (FLC). In addition, the proposed electronic differential system provides robust control of the scooter on the road. It also allows controlling autonomously each drive wheel to roll at different speeds.

Modeling and simulations is performed by using MATLAB Simulink. Additionally, the classic PI controller is also used so as to check and evaluate the performance of the suggested FLC.

The general structure of this article is divided as follows: Part I expose the components of the traction scheme basically, while the second part presents the mathematical model of the BLDC engine and the speed control. The third part introduces the mathematical equations that represent the resistance forces of the electric scooter and also the mathematical model which represents the electronic differential. Part IV exposes the results of simulation of the system. At the final part, the simulation results and performance of the controller are presented.

## 2. Electric Scooter Traction System Elements Modeling

The electric scooter contains electronic differential, lithium ion battery, buck boost converter, inverters for left and right wheels, BLDCMs and gears. Figure1 presents the general diagram of an electric scooter traction chain [10, 11]. The traction chain of electric scooter is illustrated in Fig. 1.

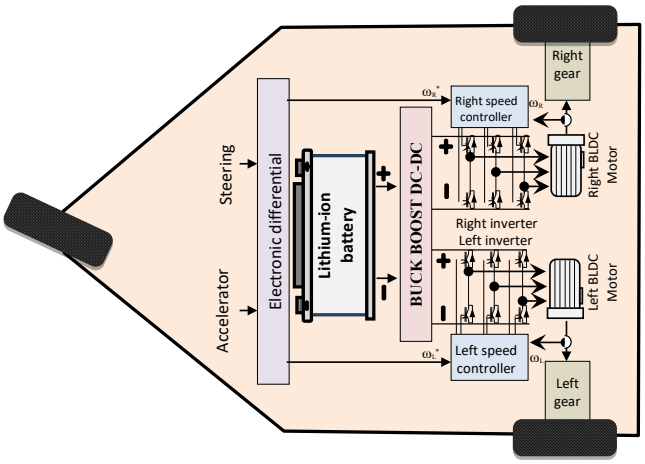


**Fig. 1.** Electric scooter traction chain.

*2.1. The Energy Source of Scooter*

Among the batteries with the most advanced technology, the li-ion battery is chosen, which is characterized by providing more energy with less weight [2, 4, 5, 7].

As shown in Table 1, the Li-ion battery has a power density of 250w / kg which is much higher than the Ni-Cd, Ni-MH and Lead Acid batteries, making the Lithium-Ion battery the most widely used in the electric scooter storage system.

The operation principle of lithium-ion battery during discharge is the transfer of lithium-ions from the anode electrolyte to the cathode material, which causes a potential difference in the charge. However, the mechanism is reflected in the case of charging the battery. Figure 2 exposes both cases.

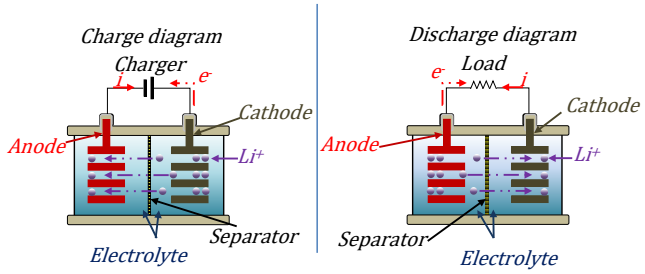


**Fig. 2**. Li-Ion battery charge and discharge diagram.

**Table 1.** The characteristics of some batteries.

| Type of Battery | Life cycle | Energy density (Wh/kg) | Power density (W/kg) | Operating temper-ature (°C) | Recharge time (hour) |
|---|---|---|---|---|---|
| Lithium ion | >1000 | 110-250 | 300-1500 | -20 to 60 | 2-3 |
| Ni-Cd | ~1200 | 45-80 | 125 | -40 to 60 | 1 |
| Ni-MH | ~1000 | 60-120 | 200 | -20 to 60 | 1 |
| Lead Acid | >800 | 30-50 | 250 | -20 to -60 | 8 |

In this study, the battery is chosen as Lithium Ion [12, 14] and Fig. 3 presents the equivalent circuit of this battery.

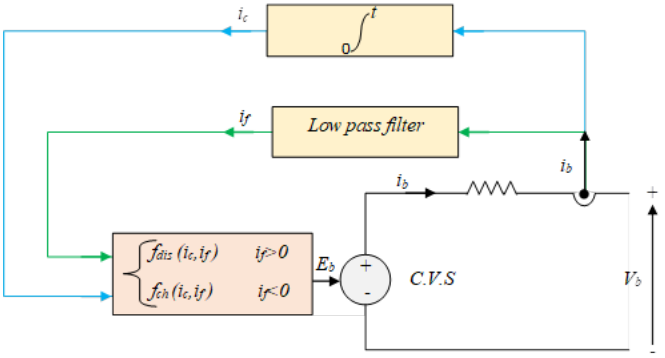


**Fig. 3.** The equivalent circuit of Li -Ion battery.

Where, $R_{int}$ is internal resistance (Ω), $E_b$ is nonlinear voltage (V), $i_b$ is battery current (A), *C.V.S.* is controlled voltage source.

The model of lithium-ion battery uses two equations:

For $i_f > 0$ (Discharge model)

$$f_{dis}(i_c, i_f) = E_0 - \frac{k \cdot Q_M}{Q_M + i_c} i_f - \frac{k \cdot Q_M}{Q_M - i_c} i_c + \alpha e^{-\beta \cdot i_c} \quad (1)$$

For $i_f < 0$ (Charge model)

$$f_{dis}(i_c, i_f) = E_0 - \frac{k \cdot Q_M}{0.1 \cdot Q_M + i_c} i_f - \frac{k \cdot Q_M}{Q_M - i_c} i_c + \alpha e^{-\beta \cdot i_c} \quad (2)$$

In the equations, $E_0$ is constant voltage (V), $k$ is steady constant (Ah), $i_f$ is low frequency current dynamics (A), $i_c$ is extorted capacity (Ah), $Q_m$ is maximum battery capacity (Ah), $\alpha$ is exponential voltage (V), $\beta$ is exponential capacity (Ah).

The SOC for a completely charged battery is 100% and for a vacuous battery is 0% [14]. The SOC is calculated through the following equation:

$$SOC = 100(1 - \frac{1}{Q_M} \int_0^t i(t)dt) \quad (3)$$

### 2.2. Buck Boost DC-DC Converter for Electric Scooter

Buck boosts DC-DC converters provide charge to the battery in recovery braking phases where backup power is needed in order to maintain the necessary storage for the specific trajectory. The power flow is moved in a bidirectional path [15, 16]. buck-boost converter of an electric vehicle supplies an output voltage that may be more or less than the input voltage of the battery [9, 14, 16].

### 2.3. Brushless DC Motors

BLDC motors may be with inner or outer rotor types. For both types are build up with permanent magnets. The total of magnetic parts is equivalent to the number of poles of the motor. The windings of phases are disseminated on the stators to the trapezoidal form BEMF [17]. Phase-Phase BEMF and the structure of the BLDCM are exposed in Figure 4.

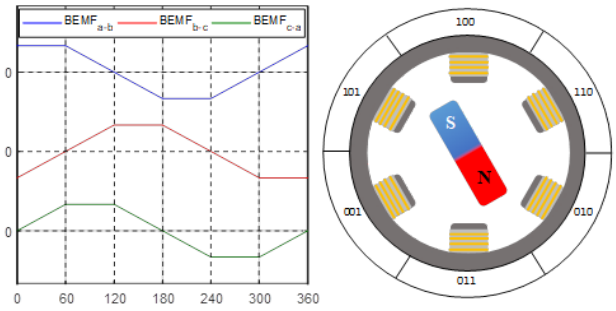


**Fig.4.** (a)Phase-phase BEMF of BLDC motor's, (b)Construction of BLDCM.

Thanks to high torque density and efficiency with quiet operation and low maintenance and tiny size of the BLDCMs, they are much suitable for steering wheel controls, electric propulsion systems, conveyor controls, etc. [17].

The mathematical model of three-phase BLDCM is described by the following equation:

$$\begin{bmatrix} v_a \\ v_b \\ v_c \end{bmatrix} = \begin{bmatrix} R & 0 & 0 \\ 0 & R & 0 \\ 0 & 0 & R \end{bmatrix} \begin{bmatrix} i_a \\ i_b \\ i_c \end{bmatrix} + \frac{d}{dt} \begin{bmatrix} L-M & 0 & 0 \\ 0 & L-M & 0 \\ 0 & 0 & L-M \end{bmatrix} \begin{bmatrix} i_a \\ i_b \\ i_c \end{bmatrix} + \begin{bmatrix} e_a \\ e_b \\ e_c \end{bmatrix} \quad (4)$$

Where $v_a$, $v_b$, $v_c$ and $i_a$, $i_b$, $i_c$ are three-phase voltages and currents, $e_a$, $e_b$, $e_c$ are phase BEMF, $R$ and $L$ are the stator resistance and inductance respectively, $M$ is the mutual inductance. In Eq.5 and Eq.6, electromagnetic and mechanical torque equations are shown. $T_L$, $j$, $\omega$, $f$ are load torque, inertia, damping and angular speed of rotor, respectively [17].

$$T_e = \frac{i_a \cdot e_a + i_b \cdot e_b + i_c \cdot e_c}{\omega} \quad (5)$$

$$j\frac{d\omega}{dt} = T_e - f \cdot \omega - T_L \quad (6)$$

### 2.4. The Design of The BLDCM Speed Controllers

The speed controllers which are applied to the BLDCM to get good performance is presented in this section. Figure 3 represents the diagram of the basic units of controller for BLDCM [6, 13].

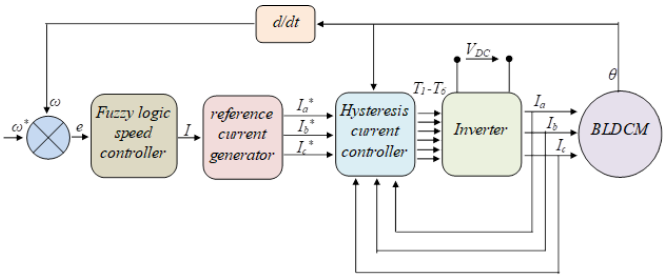


**Fig. 5.** General diagram of the control of the brushless DC motor.

### 2.5. Design of Fuzzy Logic Controller

The linguistic terms of fuzzy logic are most often expressed as logical intimations, such as If Then rules. These rules identify a variety of standards called "fuzzy membership functions". Fuzzy membership functions can have a triangle shape, a trapezoid shape and more [10, 23, 24].

The fuzzy controller calculates an error value (e) as the distinction between the reference speed and the actual speed.

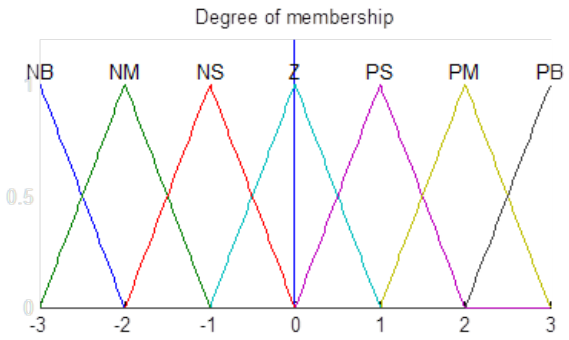


**Fig. 6.** Fuzzy membership functions

49 rules were attained depending on the number of membership functions. These rules are exposed in the Table. 2.

**Table 2.** Fuzzy rule table.

| u | | E | | | | | | |
|---|---|---|---|---|---|---|---|---|
| | | NB | NM | NS | Z | PS | PM | PB |
| de | NB | NB | NB | NM | NM | NS | NS | Z |
| | NM | NB | NM | NM | NS | NS | Z | PS |
| | NS | NM | NM | NS | NS | Z | PS | PS |
| | Z | NM | NS | NS | Z | PS | PS | PM |
| | PS | NS | NS | Z | PS | PS | PM | PM |
| | PM | NS | Z | PS | PS | PM | PM | PB |
| | PB | Z | PS | PS | PM | PM | PB | PB |

Where: de(t) and u are the error speed variation and output control respectively.

In the meantime, the membership function and its discretization are the primary ones to be qualified. The corresponding quantitative input field is defined as {-3, -2, -1, 0, 1, 2, 3} and {-3, -2, -1, 0, 1, 2, 3} as shown in Figure 7 and Figure 8.

The output field is selected as {-3, -2, -1, 0, 1, 2, 3}. The suggested membership function is shown in Figure 9.

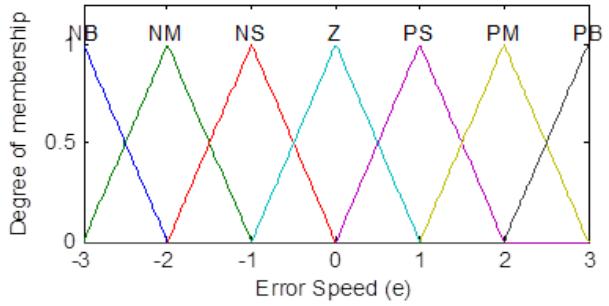


**Fig. 7.** Speed error membership functions.

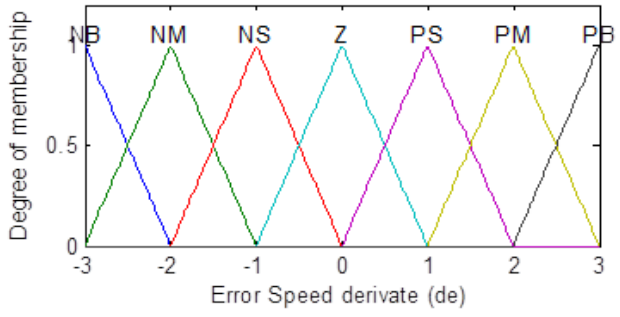


**Fig. 8.** Speed error derivate membership functions.

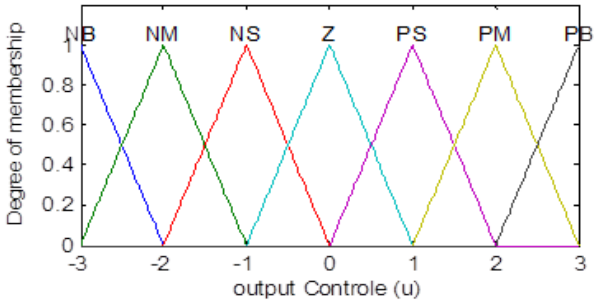


**Fig. 9.** Output control membership functions.

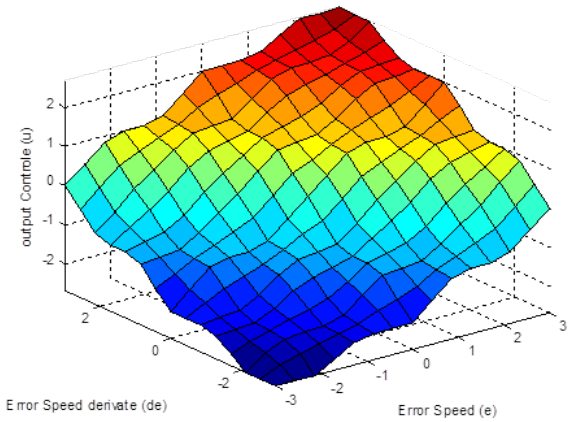


**Fig. 10.** View plot surface of fuzzy controller

## 3. Electric Scooter Mechanical Load

According to Figure 4, the opposition forces operating on the movement of the vehicle are: the rolling resistance force due to the friction of the tires of the vehicle on the road; aerodynamic drag force caused by friction on the body moving in the air; and the climbing force which depends on the slope of the road [19, 20, 23].

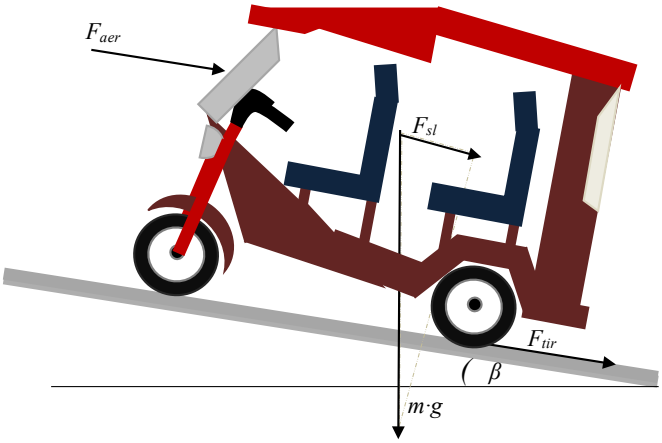


**Fig. 11.** The scooter acting forces during slope.

The scooter resistive force is equivalent to $F_r$ and it is the entire resistance forces, as in Eq. 7 [18].

$$F_r = F_{tir} + F_{aer} + F_{sl} \tag{7}$$

The rolling resistance force $F_{tir}$ is defined by [18]:

$$F_{tir} = f_r \cdot m \cdot g \tag{8}$$

The aerodynamic resistance torque $F_{aer}$ is given as [21]:

$$F_{aer} = \frac{1}{2} \cdot \rho_a \cdot s \cdot c_x \cdot V_L^2 \tag{9}$$

The slope resistance force $F_{sl}$ is usually modelled as [18]:

$$F_{sl} = m \cdot g \cdot \sin \beta \tag{10}$$

Where m is the vehicle mass, $f_r$ is the rolling resistance force constant, $g$ the gravity acceleration, $\rho_\alpha$ is the air density, $c_x$ is the aerodynamic drag coefficient, $s$ is the frontal surface area of the vehicle [19, 21, 23].

### *3.1. Gear*

The gear ensures the transmission of the engine torque to the drive wheels. This gear is modelled by using the gear ratio, the transmission efficiency and inertia [10].

The mechanical equation is defined as follows:

$$j_e \cdot \frac{d\omega}{dt} = T_e - f \cdot \omega - T_L \tag{11}$$

$$T_L = \frac{1}{\eta \cdot N_{gear}} \cdot T_r \tag{12}$$

$$J_e = J + \frac{J_s}{\eta \cdot N_{gear}^2} \cdot T_r \tag{13}$$

## 4. Scooter Electronic Differential System (EDS)

While the back wheels have the same speed and the torque on the straight road, the inner and outer wheels are not on a similar path on bend road. The traction wheels must therefore have dissimilar speeds for steady driving. Though the mechanical differential performs this task in conventional vehicles, the electronic differential is used for electric vehicle systems [24]. Figure 10 shows a scooter moving on a bend road. $R_w$, $L_w$, $d_w$ and $\delta$ are rotating radius, wheelbase, distance between driving wheels and steering angle, respectively.

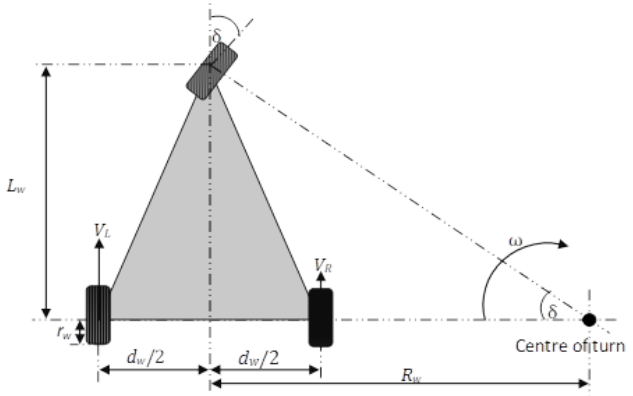


**Fig. 12.** Scooter moving on curved road.

The distinction between traction wheel angular speeds is:

$$\Delta\omega = \frac{d_w \cdot \tan\delta}{L_w} \omega^* \tag{14}$$

The speed change is being changing with adding and subtracting to/from the average value of the wheels' reference speed ($\omega^*$) to obtain each reference back angular speed ($\omega_R^*, \omega_L^*$). In the Eq.14, $\delta$ is also used for determining the trajectory. When the value of $\delta$ is lower than 0 ($\delta < 0$), it turns left. If δ is equal to 0 ($\delta = 0$), go straight. And the other situation, when the value of $\delta$ is higher than 0 ($\delta > 0$), it turns right.

## 5. Results

The EDS is simulated under the constant reference speed as 45 km/h. The topology studied in this study consists of seven phases and these are presented in Table 3. Also, the studied road topology can be shown in Figure 13.

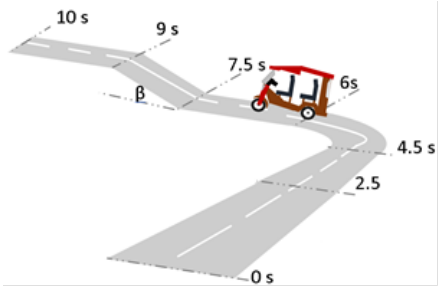


**Fig. 13.** The natural driving road

**Table 3.** Studied road topology.

| Time (s) | Phase number | Description |
|---|---|---|
| [0: 2] | 1 | straight road topology |
| [2: 4] | 2 | left curved road |
| [4: 6] | 3 | straight road driving |
| [6: 8] | 4 | the right curved road |
| [8: 10] | 5 | straight road |
| [10 :12] | 6 | the scooter moving on slope road |
| [12 :14] | 7 | the scooter moving on straight road |

Figure 13 presents the natural driving road. When a scooter follows a straight road, all wheels have the same speed but when entering a curved road, the speed of the external wheels became higher comparing with the speed of the internal wheels, as shown in Figure 14.

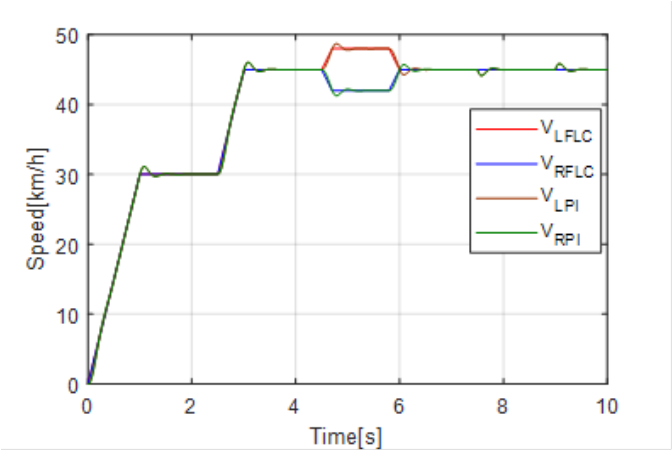


Fig. 14. Rear wheel speeds using FLC controller.

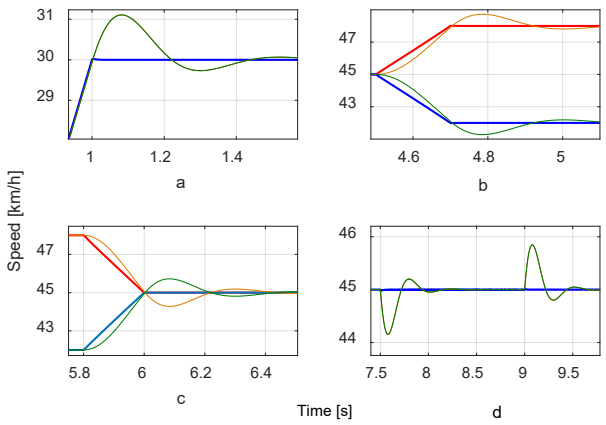


**Fig.15.** (a), (b), (c) and (d). Zoom of rear wheel speeds.

Figure 15 shows the difference in the ability to control the speed between the fuzzy logic controller and the PI controller when a scooter enters a bend or traverses a high road, causing an increase in load on the engine.

**Table 4.** The studied road topology.

| Controller | rise time [s] | settling time [s] | overshooting [%] |
|---|---|---|---|
| PI | 0.2315 | 0.4286 | 2.333 |
| FLC | 0.1234 | 0.1515 | 0.012 |

Table 4 shows the efficiency and the high power of the FLC compared to the classical PI controller by means of reducing the three indicators (rise time; settling time; overshooting) while the electric scooter is subjected to disturbances.

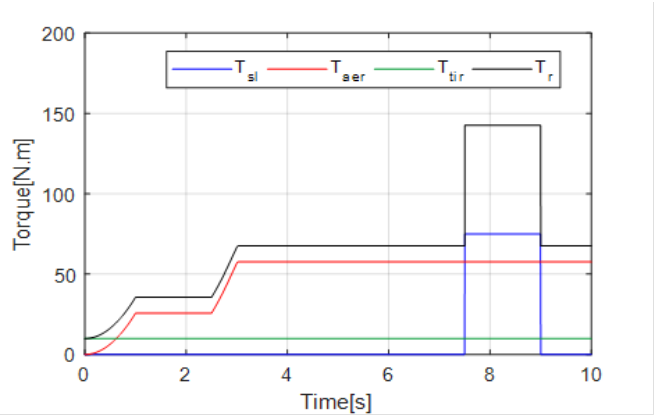


**Fig. 16.** Vehicle resistive torques

In the first stage, the scooter starts up to a speed of 30km/h which makes it subject to a resistive torque of 37Nm. In stages 2, 3 and 4, the scooter moves at a speed of 45km/h, rising the resistor torque to approximately 57Nm. In the fifth stage, the applied resistive resistance reaches 140Nm due to the entry of the scooter in a high road, causing the increase in load.

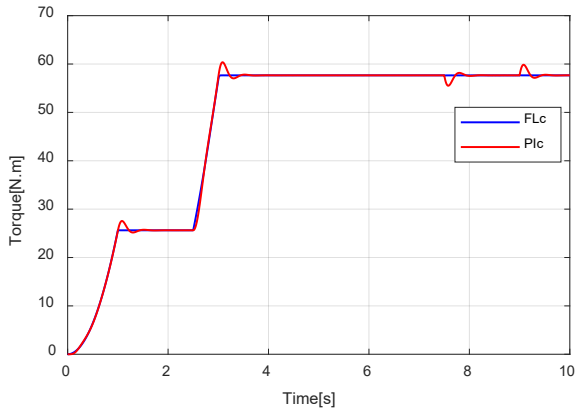


**Fig. 17.** Aerodynamic torque

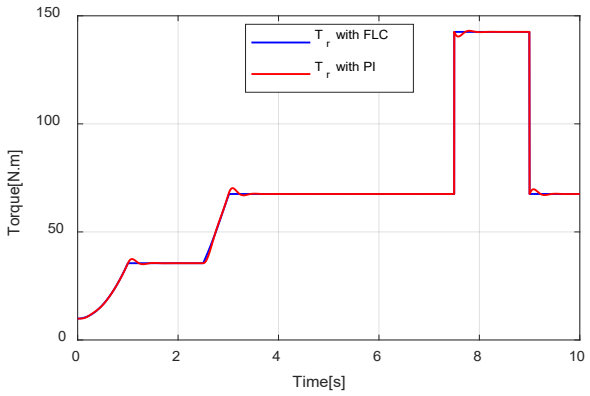


**Fig. 18.** Vehicle total resistive torques

During the application of the FLC, it provides a relatively lower dynamic torque than the torque during the application of the classical PI unit because of the applied speed to the front-facing surface (the speed of the application of the FLC less than during the application of PI) see Table 5.

Figures 19, 20 and 21 show the changes of the electromagnetic torque, the electric current of phase A of the engine's torque and the Back Electromotive Force of Phase A, respectively.

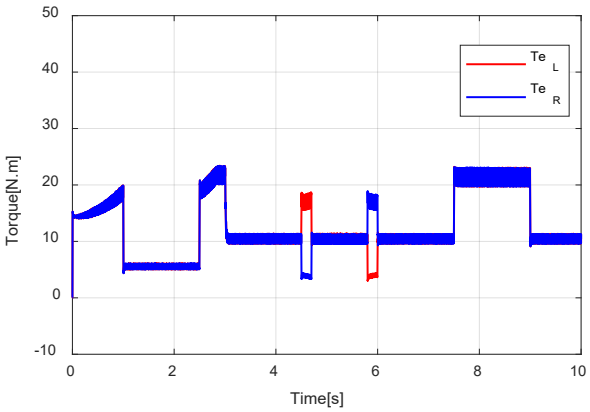


**Fig. 19.** Electromagnetic Torques

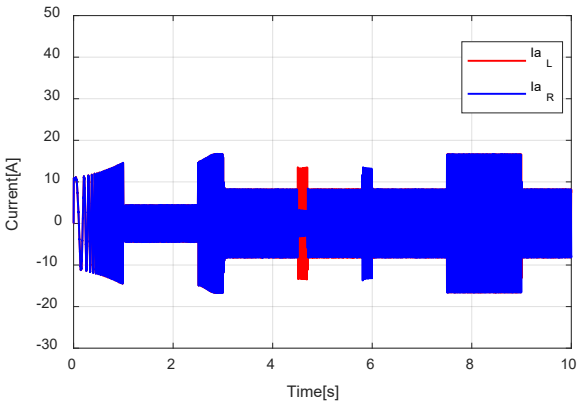


**Fig. 20.** Phase A BEMF of BLDCM

Figures 21 and 22 present the battery voltage and output voltage of Buck-Boost Converter, where it appears clear the Buck-Boost Converter ability to raise the battery voltage and maintain its stability no matter how much changes the output voltage of battery.

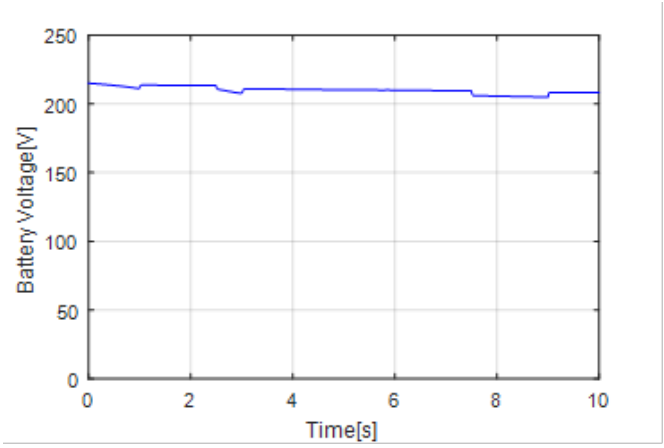


**Fig. 21.** Output voltage of battery

Table 5. Studied road topology.

| Time [s] | **Aerodynamics Torque** $T_{aer}$ [N.m] | | **Vehicle resistive Torque** $T_r$ [N.m] | |
|---|---|---|---|---|
| | PI | FLC | PI | FLC |
| 1.08 | 27.55 | 25.62 | 37.45 | 35.52 |
| 3.08 | 60.36 | 57.66 | 70.26 | 67.56 |
| 7.58 | 55.51 | 57.66 | 140.4 | 142.5 |
| 9.08 | 59.84 | 57.66 | 69.74 | 67.56 |

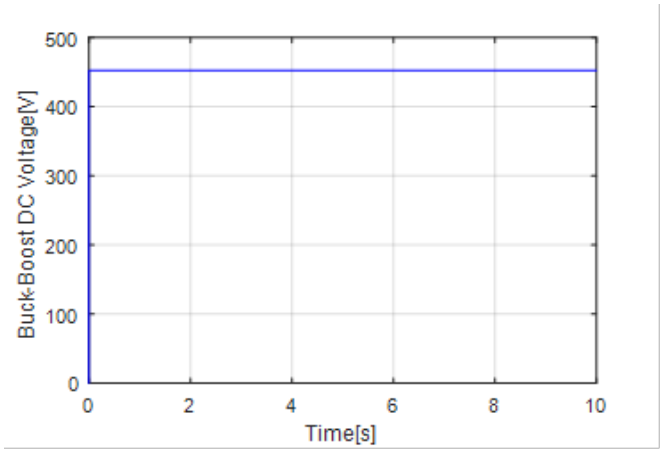


**Fig. 22.** Output voltage of buck-boost converter

Figures 23, 24 and 25 show respectively the current power, battery power, and charge status of the electric scooter while under some disturbance conditions.

The power increases while accelerating and when entering a high road, causing a raise in the use of power and a drop in the charging status.

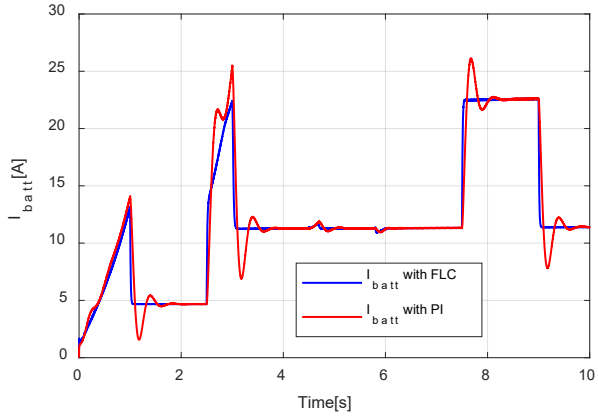


**Fig. 23.** Battery Current in Different Cases.

Figure 26 shows the distance traveled by the electric scooter in terms of time, where this scooter crosses approximately 110 meters in 10 seconds.

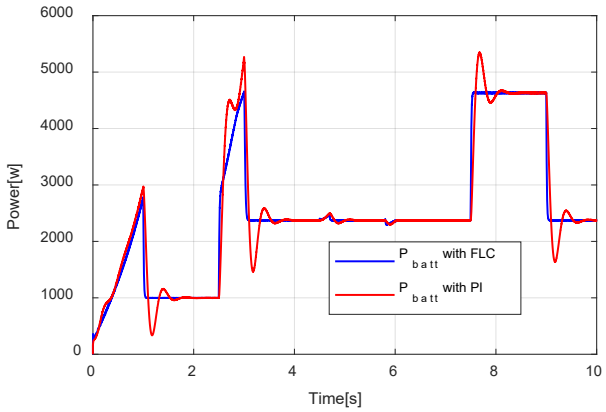


**Fig. 24.** Battery power in Different Cases.

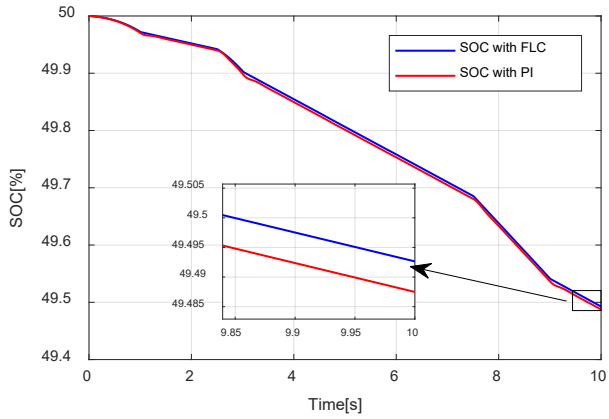


**Fig. 25.** SOC with FLC and PI Controller (%)

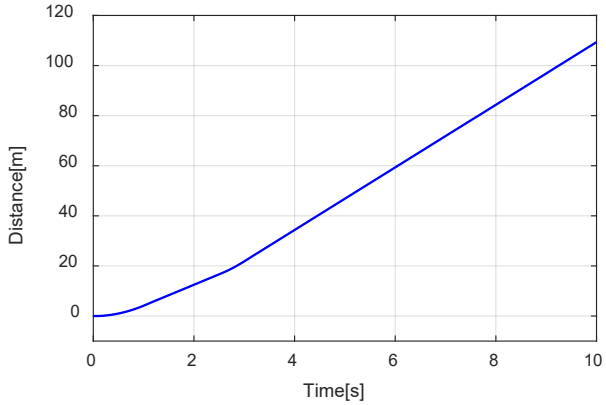


**Fig. 26.** Travelled distance

**Table 6.** Studied road topology

| Time [s] | Battery current [A] | | Battery Power Consumed [Kw] | | SOC [%] | |
|---|---|---|---|---|---|---|
| | PI | FLC | PI | FLC | PI | FLC |
| 0 | 0 | 0 | 0 | 0 | 50.000 | 50.000 |
| 1 | 14.09 | 13.15 | 2973 | 2777 | 49.970 | 49.975 |
| 3 | 25.50 | 22.43 | 5263 | 4656 | 49.898 | 49.905 |
| 7.5 | 14.29 | 22.17 | 2970 | 4557 | 49.684 | 49.679 |
| 9 | 11.80 | 19.55 | 4033 | 2451 | 49.532 | 49.538 |
| 10 | 11.39 | 11.39 | 2369 | 2369 | 49.487 | 49.493 |

## 6. Conclusion

This study proposes the "independent motor" control structure applied to the electric scooter propulsion system by a three-wheeled electric scooter used for the urban passenger guarantee by means of electronic differential. The BLDCM was used at each the rear wheels and the FLC was used to direct the rapidity of each motor.

The simulation is performed at a fixed speed with some suppositions. Comparative simulation findings were introduced with the Electronic Differential system using the PI speed controller. The suggested Electronic Differential system has a rapid response on the bend as well as ramp road. The findings of the simulation demonstrate that the suggested electronic differential system functions pleasingly.

## Appendix

**Table 7.** The parameters of electric scooter

| | | |
|---|---|---|
| $r_w$ | Wheel radius | 0.29m |
| $\eta$ | Total transmission efficiency | 93% |
| $M_S$ | Scooter mass | 230Kg |
| $S$ | Scooter frontal area | 2.09 $m^2$ |
| $f_s$ | Scooter friction coefficient | 0.01 |
| $L_w$ | Distance between the back and the front wheel | 2.4m |
| $d_w$ | Distance between two rear wheels | 1.25m |

**Table 8.** The parameters of BLDCM

| | | |
|---|---|---|
| $R$ | Stator winding resistance | 8.175 Ω |
| $L$ | Stator leakage inductance | 8.5 mH |
| $f$ | Friction coefficient | 0.001 |
| $P$ | Number of poles | 4 |

**Table 9.** Symbols, designation and Units

| Symbols | Nomenclature | Units |
|---|---|---|
| $J_e$ | Moment of inertia of the drive train | Kg.m2 |
| $J_s$ | Scooter inertia | Kg.m2 |
| $T_e$ | Electromagnetic torque | Nm |
| $T_r$ | Total resistance torque | Nm |
| $T_{sl}$ | Slope torque | Nm |
| $T_{aer}$ | Aero-dynamic torque | Nm |
| $T_{tir}$ | Tire torque | Nm |
| $BEMF$ | Back Electromotive Force | V |
| $N_{gear}$ | Report of speed gear | % |
| $g$ | Gravitational acceleration | N/m |
| $V_h$ | Vehicle linear speed | Km/h |
| $\Delta\omega$ | Angular speed variation given by electronic differential | Rad/sec |
| $\omega_R$ | Right wheel angular speed | Rad/sec |
| $\omega_R$ | Left wheel angular speed | Rad/sec |
| $\beta$ | Vehicle slop angle | rad |
| $FLC$ | Fuzzy logic controller | |
| $PI$ | Proportional Integral | |

**References**

[1] F. Caricch, L. Del, G. F. Capponi, O. Honorati, E. Santini, "Three-wheeled electric maxi-scooter for improved driving performances in large urban areas", Electric Machines and Drives Conference, Dept. of Electr. Eng., Rome Univ., Italy, 2003.

[2] A. M. Mlayah, & A. Khedher, "Sliding Mode Control Strategy for Solar Charging of High Energy Lithium Batteries", International Journal of Renewable Energy Research (IJRER), 8(3), 1621-1630, 2018.

[3] J. Hollingsworth, B. Copeland, J. X. Johnson, "Are e-scooters polluters? The environmental impacts of shared dockless electric scooters", Environmental Research Letters, 14(8), 084031, 2019.

[4] I. Oukkacha, M. B. Camara, & B. Dakyo, "Energy Management in Electric Vehicle based on Frequency sharing approach, using Fuel cells, Lithium batteries and Supercapacitors", In 2018 7th International Conference on Renewable Energy Research and Applications (ICRERA) (pp. 986-992). IEEE.

[5] Y. W. Chen, C. Y. Cheng, S. F. Li, C. H. Yu, "Location optimization for multiple types of charging stations for electric scooters", Applied Soft Computing, 67, 519-528, 2018.

[6] C. C. Chang, F. L. Wu, W. H. Lai, M. P. Lai, "A cost-benefit analysis of the carbon footprint with hydrogen scooters and electric scooters", International Journal of Hydrogen Energy, 41(30), 13299-13307, 2016.

[7] P. Y. Hsieh, T. Y. Yu, K. C. Wu, L. F. W. Chang, "Influences and uncertainty of battery-swapping electric scooters on energy system in Taiwan", Energy Procedia, 153, 95-100, 2018.

[8] C. L. Lin, M. Y. Yang, E. P. Chen, Y. C. Chen, W. C. Yu, "Antilock braking control system for electric vehicles", The Journal of Engineering, 2018(2), 60-67, 2018.

[9] M. E. Sahin, & H. I. Okumus, "Small signal analyses and hardware implementation of a buck-boost converter for renewable energy applications", In 2013 International Conference on Renewable Energy Research and Applications (ICRERA) (pp. 330-335). IEEE.

[10] A. Nasri, A. Hazzab, I.K. Bousserhane, S. Hadjeri and P. Sicard, "Two Wheel Speed Robust Sliding Mode Control For," Serbian Journal of Electrical, vol. 5, no. 2, pp. 199-216, 2008.

[11] A. Nasri, A. Hazzab, I.K. Bousserhance, S. Hadjeri and P. Sicard, "Fuzzy-Sliding Mode Speed Control for Two Wheels Electric Vehicle Drive," Korean Journal of Electrical Engineering & Technology, vol. 4, no. 4, pp. 499-509, 2009.

[12] Il. Song. Kim, "Non-Linear State of Charge Estimator for Hybrid Electric Vehicle Battery," IEEE Transactions, vol. 23, no. 4, pp. 2027-2034, 2008.

[13] S. Tsotoulidis, A. Safacas, &, E. Mitronikas, "Multiresolution PID control of brushless DC motor in fuel cell electric vehicles", In 2013 International Conference on Renewable Energy Research and Applications (ICRERA) (pp. 611-616). IEEE.

[14] A. Nasri and G. Brahim, "A Novel Lithium Ion Battery Autonomous Strategy Improvement Based on SVM-DTC for Urban Electric Vehicle under Several Speeds Tests," Majlesi Journal of Electrical Engineering, vol. 5, no. 4, pp. 41-45, 2011.

[15] C. Xia and Y. Guo, "Implementation of a Bi-directionalDC/DC Converter in the Electric Vehicle," Journal ofPower Electronics, vol. 40, no. 1, pp. 70-72, 2006.

[16] Q. Zhang and Y. Yin, "Analysis and Evaluation of Bidirectional DC/DC Converter," Journal of Power Technology, vol. 1, no. 4, pp. 331–338, 2003.

[17] H. Kahveci and I. O. Halil, "An Electronic Differential System Using Fuzzy Logic Speed Controlled In-Wheel Brushless DC Motors," in Power Engineering, Energy and Electrical Drives, Istanbul, Turkey, 2013.

[18] A. Damiano, C. Musio, & I. Marongiu, "Experimental validation of a dynamic energy model of a battery electric vehicle", In 2015 International Conference on Renewable Energy Research and Applications (ICRERA) (pp. 803-808). IEEE.

[19] Y.P. Yang and C. Lo, "Current Distribution Control of Dual Directly Driven Wheel Motors for Electric Vehicles," Control Engineering Practice, vol. 16, no. 11, pp. 1285-1292, 2008.

[20] M. R. Jiménez,. "Analysis for the design of a unipersonal electric vehicle prototype with photovoltaic panels". In 2014 III International Congress of Engineering Mechatronics and Automation (CIIMA) (pp. 1-5). IEEE.

[21] P. He, Y. Hori, M. Kamachi, K. Walters and H. Yoshida, "Future Motion Control to be Realized by In-wheel Motored Electric Vehicle," in the IEE Industrial Electronics Society, IEEE Press, Raliegh South Carolina, 2005.

[22] B. Gasbaoui, A. Nasri, M. Rahli And A. Chaker, "An Intelligent PI Speed Controller for 4WD Urban Electric Vehicle," ELECTROTEHNICÃ, ELECTRONICÃ, AUTOMATICÃ, vol. 62, no. 2, pp. 30-38, 2014.

[23] B. Allaoua, A. Laoufi, and A. Nasri, “Intelligent Controller design of DC motor speed control based on Fuzzy Logic -Genetic Algorithms Optimisations,” Leonardo Journal of Sciences, Issue 13, Dec., pp.90-102, 2008.

[24] A. Nasri, A. Hazzab, I. Bousserhane, S. Hadjeri and P. Sicard, “Fuzzy Logic Speed Control Stability Improvement of Lightweight Electric Vehicle Drive” Journal of Electrical Engineering & Technology, vol. 5, n1, pp. 129-139, 2010.